Natural Resources Canada | Ressources naturelles Canada

GEOLOGICAL SURVEY OF CANADA
OPEN FILE 9324e

Hydrochemical variability in subarctic lakes near Rankin Inlet, Nunavut: insights from the ice-off period

B.F. Faucher, A.-M. LeBlanc, J.A. Kidder, N. Benoit, É. Girard, D. Lacelle, and B. Voth

2026

Canada

GEOLOGICAL SURVEY OF CANADA
OPEN FILE 9324e

Hydrochemical variability in subarctic lakes near Rankin Inlet, Nunavut: insights from the ice-off period

B.F. Faucher[1], A.-M. LeBlanc[1], J.A. Kidder[1], N. Benoit[2], É. Girard[2], D. Lacelle[3],and B. Voth[3]

[1]Natural Resources Canada, Geological Survey of Canada, 601 Booth Street, Ottawa, Ontario K1A 0E8
[2]Natural Resources Canada, Geological Survey of Canada, 490 rue de la Couronne, Québec, Quebec G1K 9A9
[3]Department of Geography, Environment and Geomatics, University of Ottawa, 60 University Private, Ottawa, Ontario K1N 6N5

2026

Recommended citation
Faucher, B.F., LeBlanc, A.-M., Kidder, J.A., Benoit, N., Girard, É, Lacelle, D., and Voth, B., 2026. Hydrochemical variability in subarctic lakes near Rankin Inlet, Nunavut: insights from the ice-off period; Geological Survey of Canada, Open File 9324e, 23 p. https://doi.org/10.4095/ppdr59a3b4

Publications in this series have not been edited; they are released as submitted by the author.

ISSN 2816-7155
ISBN 978-0-660-97947-2
Catalogue No. M183-2/9324E-PDF
https://doi.org/10.4095/ppdr59a3b4

Hydrochemical variability in Subarctic lakes near Rankin Inlet, Nunavut: insights from the ice-off period

Benoit Faucher[1], Anne-Marie LeBlanc[1], James Kidder[1], Nicolas Benoit[2], Étienne Girard[2], Denis Lacelle[3] and Benjamin Voth[3]

[1]Natural Resources Canada (Geological Survey of Canada), 601 Booth Street, Ottawa (ON)

[2]Natural Resources Canada (Geological Survey of Canada), 490 rue de la Couronne, Québec (QC)

[3]University of Ottawa (Department of Geography, Environment and Geomatics), 60 University Pr., Ottawa (ON)

SUMMARY

Groundwater inflows via lake taliks are hard to trace in northern lakes. Our previously published physicochemical profiles from September 2023 showed Rankin Inlet (Nunavut) lakes to be fully polymictic during the ice-off season, meaning that any groundwater signal present would then be rapidly diluted, unlike during the ice-on period, when thermal stratification could preserve such a groundwater input signal. To determine whether any groundwater signal persists through ice-off mixing and to build a hydrochemical baseline, we analyzed 1 m, 5 m, and near-bottom water samples from the same lakes profiled in September 2023. Samples were analyzed for major ions, δ^2H-δ^{18}O, δ^{13}C-TIC, δ^{34}S-SO_4, and ^{3}H. δ^2H-δ^{18}O values plotted below the local meteoric water line, with the smallest lakes being the most evaporatively enriched. Tritium ranged between 9.9 and 11.8 TU, matching modern precipitation data from Churchill (Manitoba). δ^{13}C-TIC (-7.2 to -3.5 ‰) likely reflected carbonate buffering, while δ^{34}S-SO_4 (0.7-16.7 ‰) pointed to a sedimentary or marine sulphate origin. Three geochemical facies emerged: Ca-HCO_3, Ca-Cl, and high-TDS Na-Cl confined to a few near-bottom samples. Weathering models of tills intermixed with marine sediments could not reproduce the elevated Na/Cl and low Ca/Cl ratios in the lake water samples, suggesting additional controls (e.g., evaporation, cation exchange, permafrost degradation, leaching of marine deposits, groundwater inflow). Overall, this study delivers a first hydrochemical baseline for several lakes situated near Rankin Inlet and confirms that talik-derived groundwater is difficult to detect during the ice-off polymictic season; winter, stratified sampling is needed to isolate such inputs.

INTRODUCTION

Lakes across the Arctic and Sub-Arctic rapidly respond to environmental changes, making them sensitive indicators of shifting climate and permafrost conditions (Goldman et al., 2012). Shaped mainly by glacial or thermokarst processes, these waterbodies endure long ice-on periods, brief ice-off seasons, and occupy landscapes underlain by perennially cryotic ground (i.e., permafrost). These unique conditions significantly affect nutrient cycling, light availability, water column dynamics, and gas exchange processes, resulting in distinctive hydrochemical and geochemical characteristics (Muster et al., 2017). Further, during the ice-off season, the water column of many northern lakes (≤ ~20 m deep) becomes fully mixed within hours, days or weeks (polymictic), producing vertically homogeneous water columns that can mask geochemical stratification and groundwater inflows (Lesack & Marsh, 2010; Vincent et al., 2011; Hinkel et al., 2016).

In continuous-permafrost landscapes, open taliks (unfrozen zones that completely penetrate the permafrost) may connect surface waters to saline subpermafrost groundwater, altering lake levels and chemistry and complicating mine-dewatering plans. Using archived surface samples, Faucher

et al. (2022) recently explored the chemical composition of surface waters from lakes situated in the Rankin Inlet area of Nunavut, identifying statistically significant differences between lakes likely hosting sublacustrine open taliks (i.e., unfrozen ground zones that completely penetrate the permafrost), from those whose talik configuration is uncertain. While these findings suggested possible groundwater inputs, the observed chemical differences between lake types were also strongly influenced by water-rock interactions and evaporation, demonstrating the complexity of distinguishing groundwater influences solely from ice-off season data, especially when only surface samples are available. All in all, this study emphasized the need to acquire further empirical data at depth, within the water column of lakes of interest, particularly hydrochemical and isotopic analyses, to better characterize groundwater inputs in lentic basins of the area.

Addressing that need, in September 2023, during the ice-off period, we (Faucher et al., 2024) first performed a physicochemical profiling of several lakes near Rankin Inlet lakes with various expected sub-lacustrine talik configurations and demonstrated that their water column was well-mixed (i.e., that they were of the cold continuous polymictic type). This led us to hypothesize that any talik-derived groundwater signal would be rapidly diluted during the ice-off season. Nonetheless, to test this hypothesis and establish an ice-off hydrochemical baseline, we collected water samples (1 m, 5 m, and near-bottom) at mostly the same sites and during the same September 2023 field campaign in which Faucher et al. (2024) conducted the water-column physicochemical surveys across several Rankin Inlet lakes. Collected lake water samples were analyzed for major ions, $\delta^{2}H$-$\delta^{18}O$, $\delta^{13}C$-TIC, $\delta^{34}S$-SO_4, and tritium (^{3}H).

Our objectives were to: 1) evaluate whether any groundwater imprint survives ice-off mixing despite documented polymixis; and 2) provide a comprehensive hydrochemical baseline for comparison with future winter (thermally stratified) data. Such a baseline is essential not only for quantifying seasonal surface-groundwater connectivity in continuous-permafrost terrain and refining talik assessments for northern resource development, but also for parameterizing the thermal, geophysical, and coupled cryo-hydrogeological models we are developing to simulate subsurface flow and the occurrence of sublacustrine open taliks within our broader multidisciplinary research project.

STUDY AREA

Geology

Rankin Inlet is situated on the western coast of Hudson Bay in the Kivalliq region of Nunavut (Canada) (Fig. 1A) within the western Churchill Province of the Canadian Shield. Its complex geology consists of Archaean Rankin Inlet Greenstone Belt felsic volcanic rocks intercalated with mafic volcanic and sedimentary rocks, and granodioritic to tonalitic intrusions (Lawley et al., 2016). Glacial, marine, and glaciofluvial deposits, including eskers, with numerous bedrock outcrops, comprise most of the surficial geological units (Geological Survey of Canada, 2017, McMartin, 2002; Fig 1B). These deposits shape a landscape characterized by low-relief terrain and elevations generally near sea level in the vicinity of the surveyed lakes. During the Wisconsin Glaciation, the Laurentide Ice Sheet covered the region and receded by ~6 kyr BP (Dyke, 2004). The postglacial Tyrrell Sea extended up to 150 km inland from the current coastline over the isostatically depressed land surface, reaching a maximum elevation of approximately 170 m above the present sea level (Dyke, 2004; McMartin et al., 2023; Randour et al., 2016).

Climate
Between 1981 and 2020, the mean annual air temperature (MAAT) for Rankin Inlet was −10.3 °C, with an average increase of 0.05 °C/year (ECCC, 2023) (Fig 2). The average total precipitation over the same period was 315 mm, with rainfall accounting for 184 mm and snow precipitations contributing 131 cm. There was no significant trend in total precipitation during the 1981 to 2020 period. The warmest year in the historical record for Rankin Inlet was 2010, which was followed by a cooling period consistent with the observed anomaly over the eastern Canadian Arctic region (Bell & Brown, 2018).

Permafrost
Continuous permafrost is ubiquitous throughout the Rankin Inlet area, except beneath large and deep lakes, where unfrozen zones (taliks) may completely penetrate the permafrost. The base of the permafrost is estimated to lie between 285 m and 430 m below the surface, with its shallowest sections typically found near large lakes (Golder, 2021). Geothermal gradients in the region have been estimated to range between 0.012 and 0.018 °C/m (Golder, 2014), while mean annual ground temperatures at the top of the permafrost vary from -9.5 to -5.5 °C. Active-layer thicknesses range from approximately 0.5 m in organic-rich alluvial-marine sediments to around 1.6 m in marine and organic-poor till deposits (LeBlanc & Oldenborger, 2021).

Water Bodies
In contrast to rarely observed thermokarst lakes, kettle lakes and lakes shaped by glaciofluvial, or glacial processes are common in the area (Golder, 2014). Those are typically seasonally ice-covered from early October to June (Golder, 2014). Their preferential orientation of the area's lakes (northwest-southeast) follows the orientation of glacial and glaciofluvial deposits. The surface area of the regional lentic water bodies ranges from 200 to 180 x 10^6 m² (Peter Lake, ~30 km northwest of the current study area) with an average and median of 71,000 and 5,400 m², respectively. Maximum depths of about 100 surveyed lakes ranged from 0.11 to 23.5 m (Golder, 2012a, 2012b). Lake expansion and drainage were attributed to thermokarst processes, observed in fine-grained and ice-rich sediments, and thickening of the active layer likely caused by the increase in subsurface water storage in coarse-grained and ice-poor sediments, respectively (LeBlanc et al., 2020).

METHODS

September 2023 water sampling
In September 2023, water column surveys and sampling were carried out remotely from the lakeshore using a *DJI Matrice 300 RTK* Unmanned Aerial Vehicle (UAV), following the methodology described in Faucher et al. (2024). A custom-designed water sampling container was suspended from the UAV using a 25-meter-long, 4 mm-thick Kevlar rope (Fig. 3). The container was equipped with a *Speedip V2 Smart Liquid Sampler*, a device specifically designed to collect water samples at discrete depths. The *Speedip* operates with a mechanism that opens at both the top and bottom during descent, allowing water to flow through, and then closes during ascent to trap water from the targeted depth. This method was successful in approximately 90 % of cases; if unsuccessful, the procedure was repeated.

Flights were conducted only under safe conditions, specifically, favorable weather and good visibility. Once airborne, the UAV followed pre-programmed flight paths to reach each sampling site, ensuring consistency across repeated measurements and facilitating reliable site revisits. At each site, the pilot manually controlled the UAV to lower the sampler into the lake at predetermined depths (typically around 1 meter, 5 meters, and near-bottom). A float affixed to the rope at the target depth enabled straightforward identification of the sampling location. For deep-water sampling, the rope was fully extended, which was sufficient given that no lake in the study exceeded 25 m in depth. To reduce the risk of UAV loss in the event the sampler became snagged, the Kevlar rope was connected to a drop mechanism, allowing the pilot to remotely release the sampling line if necessary.

Major ions

The major cations (Ca^{2+}, Mg^{2+}, Na^{+}, K^{+}) and anions (Cl^{-}, SO_4^{2-}, NO_3^{-}) analyses were undertaken at the University of Ottawa's geochemistry laboratory (Ottawa, Canada) using two separate methods. All samples for cation analysis were acidified with ultra-pure HNO_3 acid to pH of 2 before analysis on a Varian Vista-Pro inductively coupled plasma atomic emission spectrometer (ICP-AES). Anion analysis was conducted without acidification using ion chromatography through a Dionex-100 device. The analytical reproducibility was ± 5 %. Bicarbonate (HCO_3^{-}) concentrations were estimated via a mass balance approach of cations vs. anions concentrations in meq/L^{-1}.

$\delta^{18}O$ and $\delta^{2}H$ of water

The $^{18}O/^{16}O$ and D/H ratios of the lake water samples were determined at the University of Ottawa's Cryolab for Arctic, Antarctic and Planetary Studies using a Los Gatos Research liquid water analyzer coupled to a CTC LC-PAL autosampler for simultaneous $^{18}O/^{16}O$ and D/H ratio measurements of H_2O and verified for spectral interference contamination. The results are presented using the δ-notation ($\delta^{18}O$ and δD), where δ represents the parts per thousand differences for $^{18}O/^{16}O$ or D/H in a sample with respect to Vienna Standard Mean Ocean Water (VSMOW). Analytical reproducibility for $\delta^{18}O$ and δD is ± 0.3 ‰ and ± 1 ‰, respectively.

Tritium dating

Tritium (^3H) sample preparation and analysis were carried out at the A.E. Lalonde Tritium and Radiohalide Laboratories (University of Ottawa) using electrolytic enrichment followed by liquid scintillation counting. Before enrichment, the samples were de-ionized with an ion-exchange resin and shaken for four hours. The de-ionized water was then combined with sodium peroxide (Na_2O_2) and electrolytically enriched in metal cells. Enrichment occurred over five days at approximately 5.8 amps, reducing each 250 mL sample to about 13 mL. The enriched aliquots were subsequently decay-counted on a low-background Quantilus liquid scintillation counter. Tritium concentrations are reported in tritium units (TU), where 1 TU corresponds to 1 ^3H atom per 10^{18} ^1H atoms, or 0.11919 Bq/L. Calibration was performed by the A.E. Lalonde Tritium and Radiohalide laboratory staff using the certified ^3H radioactivity standard SRM–4926E.

$\delta^{13}C$ of total inorganic carbon ($^{13}C_{TIC}$)

The $\delta^{13}C$ of Total Inorganic Carbon ($^{13}C_{TIC}$) in lake water samples collected in well-sealed 40ml amber glass bottles was measured at the Ján Veizer Stable Isotope Laboratory, University Ottawa,

using methods described by St-Jean (2003). The 2sigma analytical precision is +/- 0.4 permil (‰).

^{34}S-SO_4

The $\delta^{34}S$ isotopic measurements of dissolved SO_4^{2-} was undertaken at the Jan Veizer Stable Isotope Laboratory. Samples containing sufficient SO_4^{2-} were analysed for $\delta^{34}S$ after precipitating the SO_4^{2-} into $BaSO_4$ using BaCl. Filtered $BaSO_4$ precipitates were loaded into 10x10 mm tin capsules along with WO_3 to facilitate complete combustion. Prepared samples are then flash combusted at 1800 ˚C in an Elementar Elemental Analyser Isotope Cube in S mode and SO_2 separated using a purge and trap column. $\delta^{34}S$ is then determined using a ThermoFinnigan Delta Plus XP isotope ratio mass spectrometer with a conflo IV interface. $\delta^{34}S$ values are reported relative to the Vienna Canyon Diablo Troilite (VCDT) using the delta (δ) notation in units of permil and are reproducible to 0.3 ‰.

Numerical simulations of hydrochemical processes

Two numerical models of natural processes that could shape the sampled lakes' hydrochemistry were run in PHREEQC (Parkhurst and Appelo, 2013).

The first simulated evaporation and its effect on stable water isotope ratios (δ^2H-$\delta^{18}O$). Lacking local precipitation data, we used Little Meliadine Lake (the largest and deepest sampled lake) as the starting composition (δ^2H = -115 ‰; $\delta^{18}O$ = -14 ‰). We hypothesized that its long residence time likely dampens evaporative enrichment, and so its isotopic signature is expected to lie closest to local meteoric water, making it a reasonable proxy for precipitation in the absence of direct data. The lake was treated as a closed system in which successive fractions of water were removed while applying equilibrium liquid-vapour fractionation factors (Rayleigh distillation). No inflow was allowed, so the output curve represents a pure-evaporation trajectory for ice-off conditions. Plotting measured lake-water values against this evaporation line helps reveal deviations arising from hydrological influences beyond simple water loss, thereby pointing to other sources or sinks affecting the system.

Given that most lakes in the study area overlie glacial diamicton (till) deposits intermixed with marine sediments, the goal of the second modelling exercise was to evaluate whether the weathering of such units could account for the measured ionic loads in the sampled lakes. Specifically, we aimed to assess whether empirical lake water chemistry aligned with modelled outputs; if not, this would suggest that additional factors beyond till weathering influenced the lakes' hydrochemical characteristics.

The model assumes an initial water composition based on snow chemistry from the nearby Saqvaqjuac research site (63°39′N, 90°39′W; Welch & Legault, 1986), equilibrated with atmospheric CO_2 ($pCO_2 = 10^{-3.43}$ atm), and includes 1% seawater (Millero et al., 2008) to simulate marine aerosol inputs common in coastal Subarctic environments (Vet et al., 2014). Then, we reacted the previously described initial lake water composition with three till assemblages representative of local deposits (granite-rich, greenstone-rich, and a mix of the two) whose mineralogy (McMartin, 2000) also incorporates carbonate and evaporite phases inherited from Tyrrell Sea sediments. Model outputs were then compared with observed lake chemistries to determine whether till weathering alone could reproduce the measured molar Na/Cl, Ca/Cl, and

HCO_3/Cl ratios. Although simplified, this approach provides a baseline for assessing the additional roles of other factors (e.g., evaporation, cation exchange, permafrost degradation, leaching of marine deposits, groundwater inflow) on the lakes' major ion loading.

RESULTS

The hydrochemical variability, at different depths, of the well-mixed water columns at the time of sampling in September 2023 from one or multiple sites across several lakes near Rankin Inlet, Nunavut, is presented in Table 1. A detailed presentation and interpretation of the physicochemical conditions observed during the sampling campaign are provided in Faucher et al. (2024).

Water temperature at the time of sampling ranged from approximately 6.9 to 10.1 °C at the surface and 7.6 to 8.9 °C near the bottom. In larger and deeper lakes (e.g., LML, FLL, SLL), surface temperatures generally ranged from 6.9 to 9.5 °C, and near-bottom temperatures from 7.6 to 8.7 °C. In smaller or shallower lakes (e.g., Lakes A to E), surface temperatures were typically higher, ranging from 7.0 to 10.1 °C, and near-bottom temperatures ranged from 7.8 to 8.9 °C. Measured pH values varied from 6.4 to 8.1 across all sites. In larger lakes, pH generally ranged from 6.4 to 7.6, while in smaller lakes, values extended slightly higher, up to 8.1, with the maximum observed in Lake E (Site 21).

Stable water isotope (δD-$\delta^{18}O$) measurements across the lakes showed $\delta^{18}O$ values ranging from -14.5 to -10.9 ‰ and d-excess values between -11 and +1 ‰ (Fig. 4). Most surface and near-bottom samples exhibited minor differences in isotope ratios. Near-bottom waters at Site 20 in Lake C were more enriched ($\delta^{18}O$ of -11.7‰ at 1 m vs. $\delta^{18}O$ = -10.9‰ at 3.1 m) than its surface layer. All lake-water samples plotted below the Global and Local Meteoric Water Lines (GMWL, LMWL; Fig. 4). Among the deeper lakes (i.e., LML, FLL, SLL), $\delta^{18}O$ values ranged from -14.5 to -12.6 ‰, with d-excess values between -6 and +1 ‰. In contrast, shallower lakes (Lakes A-E) showed $\delta^{18}O$ values from -12.4 to -10.9 ‰ and d-excess values from -11 to -4.3 ‰.

The main geochemical facies identified across sampled lakes were either Ca-HCO_3, mixed-type, or Na-Cl (Fig. 5). Lakes exhibiting Ca-HCO_3 facies, such as Lake D, typically displayed the lowest concentrations of major ions. In contrast, lakes characterized by Na-Cl facies exhibited elevated concentrations of major ions, notably in the near-bottom waters of Lake B (Site 6), Lake E (Site 21), and Lake C (Site 20). At Site 20, this vertical chemical contrast was especially pronounced, with surface waters showing Ca-HCO_3 signatures and bottom waters exhibiting significantly elevated Na-Cl concentrations. Overall, major ion concentrations remained relatively consistent between surface and bottom waters within individual lakes. Chloride (Cl^-) ranged widely from ~13 mg/L to a maximum of 1668 mg/L observed in the deep waters of Lake C (S20-nb). Sulfate (SO_4^{2-}) concentrations varied from 2.9 to 172 mg/L, bicarbonate (HCO_3^-) ranged typically between 20 and 45 mg/L, while calcium (Ca^{2+}) concentrations ranged mostly from 11 to 19 mg/L, reaching a maximum of 54 mg/L at depth in Lake C. Sodium (Na^+) concentrations generally spanned from ~6 to 15 mg/L, but exceeded 700 mg/L at the bottom of Lake C. Magnesium (Mg^{2+}) and potassium (K^+) concentrations typically fell between 1 and 3 mg/L, with exceptional concentrations of 94 mg/L and 24 mg/L, respectively, at depth in Lake C.

Geochemical simulations (PHREEQC) showed that weathering of local tills (granite-rich, greenstone-rich, and mixed granite-greenstone scenarios) produced solutions markedly different from observed lake waters. The granite-rich scenario resulted in extremely low Na/Cl ratios

(~10^{-9}), very low Ca/Cl ratios (~3×10^{-3}), and moderate alkalinity (HCO_3/Cl = ~0.51). The greenstone-rich till scenario yielded relatively higher Na/Cl (≈ 0.87) and Ca/Cl (≈ 0.43), but limited alkalinity ($HCO_3/Cl \approx 0.11$). The mixed granite-greenstone simulation produced highly alkaline water ($HCO_3/Cl \approx 2.34$) but negligible amounts of Na^+ and Ca^{2+}. Lake water samples showed Na/Cl ratios clustered around the seawater benchmark of 0.86 (range: 0.75-1.10), Ca/Cl ratios from ~0.03 to 0.9, and HCO_3/Cl ratios rarely exceeding 1.7.

Tritium (^3H) concentrations ranged approximately from 9.9 to 11.8 TU, with minimal vertical variation within individual lakes, closely resembling values previously reported for precipitation at Churchill, Manitoba (~600 km southeast; Terzer-Wassmuth et al., 2022). Carbon isotope (δ^{13}_{TIC}) values varied from -7.2 to -3.5 ‰ across all lakes, while sulfur isotopes of dissolved sulfate ($\delta^{34}S\text{-}SO_4$) in near-bottom waters ranged broadly from 0.7 to 16.7 ‰, with notably higher $\delta^{34}S\text{-}SO_4$ observed in smaller lakes such as Lake E (Site 21).

DISCUSSION

Tritium (^3H) dating and stable water isotopes (δD-$\delta^{18}O$): water origin perspectives

Tritium (^3H) measurements suggest that contemporary precipitation is the primary recharge source for lakes in the study area, at least during the ice-off period. This interpretation is supported by the similarity of δD-$\delta^{18}O$ values between surface and near-bottom samples (Fig. 4), indicating that the water columns were well mixed at the time of sampling. Consequently, although tritium was only measured in near-bottom samples at some sites, concentrations are likely representative of the entire water column during the ice-off period.

All lake samples plotted below the global and local meteoric water lines (GMWL, LMWL; Fig. 4), indicating that their isotopic signatures were influenced by evaporation (Skrzypek et al., 2015). Further, variability in terms of isotope values among lakes likely reflects differences in residence time driven by lake size (and associated water volume). Smaller, shallower lakes (Lakes A to E) tend to undergo faster isotopic enrichment due to stronger evaporative effects and limited mixing, making them more responsive to recent precipitation during the ice-off period. Hence, one would expect the δD-$\delta^{18}O$ values of water in those lakes to closely reflect recent precipitation events near the time of late-summer sampling. In contrast, larger and deeper lakes such as Little Meliadine Lake (LML) and First Lake (FLL) integrate inputs over longer timescales. This is probably why they exhibited comparatively less enriched $\delta^{18}O$ and δD values (Gibson, 2002). These interpretations are consistent with our evaporation modelling, where isotopic values for LML and FLL align with predicted evaporation trajectories. While smaller lakes also plot near the modelled evaporation line, they show a distinct rightward shift in thisisotopic space, suggesting stronger evaporative effects and possibly the influence of additional processes such as recent rainfall inputs or non-steady state conditions (Turner et al., 2014). More targeted, lake-specific studies that incorporate isotope data from inflows, outflows, and precipitations are warranted to refine these interpretations.

Of noteworthy mention is Site 20 (Lake C), where near-bottom waters were more enriched in $\delta^{18}O$ and δD than surface waters. This vertical pattern contrasts with expectations, as kinetic fractionation during surface evaporation typically results in enriched surface layers. Given Lake C's small size and moderate depth (~3.1 m), it would be expected to mix fully (on a daily/weekly basis) during the ice-free season, like the other cold, continuously polymictic lakes sampled. The enrichment at depth may therefore indicate contributions from water sources with

isotopic signatures distinct from those of contemporary precipitation. Although its surface area places it below the threshold for potentially hosting a sublacustrine open talik (LeBlanc et al., 2022), the lake's depth may still be sufficient to sustain unfrozen ground beneath the lakebed. As such, the presence of an open talik and associated interactions with isotopically distinct groundwaters cannot be excluded. Still, tritium counting of bottom waters at that site yielded a value of 10.8 TU, which falls within the range of recent precipitations in the area, meaning that old, subpermafrost groundwater is seemingly not feeding the lake. Instead, degradation of permafrost around Lake C could be the main driver for the presence of isotopically distinct waters at site 20. Bellehumeur-Génier et al. (2017) documented a 2.5% increase in Lake C's surface area between 1954 and 2014, with notable expansion observed in 2005 and continuing through 2014. Updated mapping indicates that by 2023, the lake's area had increased by an additional 0.5% relative to its 1954 extent. Active thermokarst processes and permafrost thaw, evidenced by localized shoreline disturbances, have been observed in recent years at Lakes C and D, both situated within the T.M. unit (LeBlanc et al., 2020). Waters released through lateral runoff or active layer deepening may exhibit different stable isotope signatures than contemporary precipitation. The fact that this enriched signal is observed only in bottom waters suggests that such inputs may sink to the lake bottom upon entry, possibly due to their lower temperature or higher density.

Origin of dissolved ions

The mismatch between simulated weathering scenarios and measured lake chemistries highlights that weathering of local tills alone is insufficient to fully explain the hydrochemical patterns observed in lakes near Rankin Inlet. While till-weathering predominantly contributes calcium and bicarbonate, it cannot reproduce the sampled lakes' molar Na/Cl ratios (0.75-1.10), which are close to the marine benchmark of 0.86. Instead, multiple non-exclusive scenarios could explain the lake waters' Na/Cl ratios.

First, remnant Tyrrell Sea salts (primarily halite) intermixed with the various surficial geology units in the area in regional tills and marine shoreline sediments may likely contribute brines with Na/Cl ratios near 1.0. Subsequent selective removal of sodium through cation exchange onto clay minerals could readily lower this ratio toward the observed marine benchmark of 0.86. Further, marine aerosols transported inland by onshore winds from the Hudson Bay (that may come from the east or southeast during the open-water season; ECCC, 2017) could seasonally deposit salts onto the snowpack. Upon spring melt, this aerosol-derived input could reinforce the marine Na-Cl facies of some of the sampled lakes, further stabilizing lake waters within the near-marine Na/Cl ratio range. A more local source may arise from contributions linked to permafrost thaw. As saline permafrost thaws, brine-rich porewaters can drain laterally from the lake margins or rise through open taliks beneath the basins. The pronounced Na-Cl enrichment and density stratification observed in the bottom waters of Lake C (Site 20) are consistent with an influx of solute-rich porewater. However, its tritium content (10.8 TU) matches modern precipitation, indicating that the inflowing water is young and derived from thawing, near-surface sediments rather than from old, tritium-dead groundwater beneath the permafrost. These observations point to a solute flux derived from degrading permafrost. Many sediments in the area are mixed with marine material, so the dissolved ions released during degradation are likely enriched in Na^+ and Cl^-. Such salt inputs could impart a distinct Na-Cl facies to the deeper parts of the lake water column especially in September, after the maximum active layer thaw period.

As pointed out above, cation exchange may remove sodium from the lake waters through cation exchange onto clay minerals. By replacing Na^+ by Ca^{2+} ions, this could also progressively lead to the development of the Ca-Cl facies observed in some of the deeper lake basins. While cation exchange with sediment porewaters has been previously proposed as a mechanism to explain the Ca-Cl facies of sub-Arctic lakes (Faucher et al., 2022), contributions from external groundwater enriched in Ca-Cl remain a possibility that cannot yet be excluded entirely.

Carbon ($\delta^{13}C_{TIC}$) and sulfur ($\delta^{34}S\text{-}SO_4$) isotopes: biogeochemical insight

Across lakes, $\delta^{13}C_{TIC}$ values showed relatively little vertical variation, generally ranging between -7.2 and -3.5 ‰. This suggests that CO_2 produced at the sediment-water interface did not accumulate appreciably in deeper waters during the ice-free season. Instead, wind-driven circulation likely dispersed most of the CO_2 generated through organic matter remineralization, maintaining relatively stable $\delta^{13}C_{TIC}$ values throughout the water column. This pattern contrasts with observations from seasonally (dimictic) stratified Arctic lakes (often between 10 and 20 m in depth), where bottom waters during the ice-on season or early spring may exhibit $\delta^{13}C_{TIC}$ values that are substantially more negative, often reaching -10 to -15 ‰ as a result of prolonged organic matter degradation and CO_2 accumulation under low-oxygen conditions (Heim et al., 2021; Quay et al., 1986; Pasche et al., 2011).

The relatively uniform $\delta^{13}C_{TIC}$ values observed here thus imply open-system conditions concerning carbon cycling at the time of sampling and argue against strong redox stratification or the presence of a persistent, isolated bottom layer receiving isotopically distinct CO_2 inputs. Suppose mineralized groundwater entered the lakes through open taliks with significant dissolved CO_2 from deep sources or the oxidation of organic-rich sediments. In that case, one might expect a more depleted $\delta^{13}C$ signal at depth. The absence of such a signal suggests that any groundwater input is either minor, well-buffered by carbonate dissolution, or rapidly mixed into the water column during the ice-off season. Carbonate-rich materials (e.g., marine shell fragments) commonly present in local surficial deposits may also buffer $\delta^{13}C_{TIC}$ by stabilizing pH and dissolved inorganic carbon concentrations.

Sulfur isotope data show $\delta^{34}S\text{-}SO_4$ values ranging from ~0.7 to 16.7 ‰, with relatively weak vertical gradients across the lakes. This lack of isotopic stratification suggests that microbial sulfate reduction (commonly associated with strong $\delta^{34}S$ enrichment in bottom waters) is either minimal or absent during the open-water season. Instead, the $\delta^{34}S\text{-}SO_4$ profiles are consistent with well-mixed water columns and point to external sulfate inputs with limited in-lake fractionation. Values exceeding ~5-6 ‰ in some lakes, particularly those with higher salinity, suggest contributions of marine-derived ions sourced from the sediments.

Possible sources of the sulfur observed include marine sulfate, local bedrock units, glacially remobilized sulfide-bearing tills, and local anthropogenic contributions. For instance, $\delta^{34}S\text{-}SO_4$ values in lake waters (median ~4.1 ‰) partially overlap with the range reported for sulfide minerals at the nearby Meliadine gold deposit (Mongeau, 2024), though the deposit's distance and glacial dispersal patterns suggest it is unlikely to be a major source. More plausibly, legacy sulfur from the Rankin Inlet Ni-Cu mine (Meldrum et al., 2001), where wind-blown tailings rich in pyrrhotite and other sulfides were dispersed before remediation, may be contributing to the $\delta^{34}S\text{-}SO_4$ signal in the water column of lakes situated in the vicinity of Rankin Inlet. Extraction of sand

and gravel from a quarry situated near Second Landing Lake may also contribute sulfate to the system, either through surface runoff and shallow subsurface flow from weathered sulfate-bearing materials, or via atmospheric deposition of dust during dry, windy conditions.

Taken together, the $\delta^{13}C_{TIC}$ and $\delta^{34}S\text{-}SO_4$ data do not provide evidence of groundwater inflows originating from an open talik. Instead, they offer a biogeochemical context in which $\delta^{34}S\text{-}SO_4$ values in some lakes suggest limited subsurface contributions from marine-derived sediments, while relatively uniform $\delta^{13}C_{TIC}$ profiles reflect open-system carbon cycling and effective vertical mixing during the ice-free season.

CONCLUSION

This investigation surveyed late-summer hydrochemical conditions in multiple lakes near Rankin Inlet (Nunavut), focusing on major ion chemistry, stable water isotopes ($\delta D\text{-}\delta^{18}O$), and carbon and sulfur isotopes ($\delta^{13}C_{TIC}$, $\delta^{34}S\text{-}SO_4$). The main takeaways from this study are:

1) Most lakes fall into Ca-HCO_3, Ca-Cl, or Na-Cl facies. While till weathering supplies Ca^{2+} and alkalinity, the near-seawater Na/Cl ratios (0.75-1.10) and elevated ion concentrations in some bottom waters (e.g., site 20) point instead to the dissolution of marine-derived salts in surrounding sediments. These inputs may be further enhanced by thaw-related release of solutes from degrading permafrost. Overall, the major ion data alone does not support subpermafrost groundwater inflows as a dominant source.

2) Stable isotopes and tritium data indicate recent meteoric inputs (rainfall and snowmelt) as the dominant water source. Isotopic signatures vary with lake size and depth, likely reflecting differing influences of evaporation.

3) $\delta^{13}C_{TIC}$ and $\delta^{34}S\text{-}SO_4$ suggest moderate signals from organic respiration and possible marine or bedrock sulfur sources.

Although our late-summer dataset provides no conclusive evidence to confirm them, inputs from sub-permafrost groundwater remain plausible in the lakes near Rankin Inlet, which we suspect may host sublacustrine open taliks; detecting those in well-mixed water columns, during the ice-off season remains quite challenging. Upcoming analyses of water-column samples collected during the ice-on season (April 2024), when lakes are thermally stratified, should facilitate the detection of subpermafrost groundwater inputs using geochemical and isotopic tracers. This seasonal comparison will refine our understanding of the hydrological and biogeochemical processes shaping these permafrost-influenced lakes and improve detection of sub-permafrost groundwater contributions via open taliks.

ACKNOWLEDGEMENTS

This research project was funded by Natural Resources Canada's GEM-GeoNorth program. This research project benefited from the logistical support of the Iqalugaarjuup Nunanga Territorial Park. We thank the local Hunters & Trappers Organization for their field assistance. We also extend our gratitude to the internal reviewer for their constructive comments.

REFERENCES

Bellehumeur-Génier, O., Oldenborger, G. A., & LeBlanc, A.-M. (2017). Historical fluctuations of lake shorelines based on geomorphological analysis in the vicinity of Rankin Inlet, Nunavut. Geological Survey of Canada, Open File 8224, 27 pp.

Bell, T., & Brown, T. (2018). From science to policy in the eastern Canadian Arctic: An Integrated Regional Impact Study (IRIS) of climate change and modernization – Synthesis and Recommendations. ArcticNet.

Dyke, A. S. (2004). An outline of North American deglaciation with emphasis on central and northern Canada. Developments in Quaternary Sciences, 2, 373–424.

Environment and Climate Change Canada (ECCC). (2017). National Marine Weather Guide – Arctic Regional Guide.

Environment and Climate Change Canada (ECCC). (2023, October 1). Historical climate data. http://climate.weather.gc.ca/

Faucher, B., et al. (2022). Assessment of physicochemical properties in lentic water bodies of the Rankin Inlet area (Nunavut) for sublacustrine open talik detection. Geological Survey of Canada, Open File 8998.

Faucher, B., et al. (2024). Physicochemical limnology of lakes in the Rankin Inlet area of Nunavut. Geological Survey of Canada, Open File 9181.

Geological Survey of Canada. (2017). Surficial geology, Rankin Inlet, Nunavut, NTS 55-K/16. Canadian Geoscience Map 68 (preliminary, Surficial Data Model v.2.2 conversion of Open File 4116), scale 1:50 000.

Gibson, J. J. (2002). A new conceptual model for predicting isotopic enrichment of lakes in seasonal climates. PAGES news, 10(2), 10–11. https://doi.org/10.22498/pages.10.2.10

Golder. (2012a). SD 7-1 Aquatics Baseline Synthesis Report, 1994 to 2009 – Meliadine Gold Project, Nunavut. Unpublished report prepared by Golder Associates Ltd. for Agnico-Eagle Mines Limited, Doc 327-1013730076 Ver. 0.

Golder. (2012b). SD 7-2 2011 Aquatic Baseline Studies – Meliadine Gold Project, Nunavut. Unpublished report prepared by Golder Associates Ltd. for Agnico-Eagle Mines Limited, Doc 246-1013730076 Ver. 0.

Golder. (2014). SD 6-1 Permafrost Thermal Regime Baseline Studies – Meliadine Gold Project. Unpublished report prepared by Golder Associates Ltd. for Agnico-Eagle Mines Limited, Doc 225-1314280007 Ver. 0.

Golder. (2021). Meliadine Extension – 2020 Thermal Assessment – Meliadine Gold Project. Unpublished report prepared by Golder Associates Ltd. for Agnico-Eagle Mines Limited, Golder Doc 20136436-815-R-Rev2-2200.

Goldman, C. R., Kumagai, M., & Robarts, R. D. (2012). Climatic Change and Global Warming of Inland Waters: Impacts and Mitigation for Ecosystems and Societies. Wiley-Blackwell.

Heim, B., Biskaborn, B. K., Opel, T., Meyer, H., Lenz, J., Fritz, M., ... & Schirrmeister, L. (2021). Carbon isotope composition of dissolved inorganic carbon in Arctic lakes: Implications for carbon cycling in permafrost regions. Biogeosciences, 18(4), 1203–1220.

Hinkel, K. M., Lenters, J. D., Lyons, W. B., & Frey, K. E. (2016). Ice-covered lake systems of the Arctic Coastal Plain, Alaska: Hydrological, chemical, and biological dynamics. Arctic Science, 2(1), 14–34.

Lawley, C. J. M., McNicoll, V., Sandeman, H., Pehrsson, S., Simard, M., Castonguay, S., Mercier-Langevin, P., & Dubé, B. (2016). Age and geological setting of the Rankin Inlet greenstone belt and its relationship to the gold endowment of the Meliadine gold district, Nunavut, Canada. Precambrian Research, 275, 1–16. https://doi.org/10.1016/j.precamres.2016.01.008

LeBlanc, A.-M., Bellehumeur-Génier, O., Oldenborger, G. A., & Short, N. (2020). Lake area and shoreline changes due to climate and permafrost-related drivers, Rankin Inlet area, Nunavut. In Summary of Activities 2019, Canada-Nunavut Geoscience Office (pp. 79–92).

LeBlanc, A.-M., Chartrand, J., & Smith, S. (2022). Regional assessment of the occurrence of taliks below Arctic lakes. Geological Survey of Canada Scientific Presentation 138. https://doi.org/10.1139/as-2022-0002

LeBlanc, A.-M., & Oldenborger, G. A. (2021). Ground temperature, active-layer thickness and ground-ice conditions in the vicinity of Rankin Inlet, Nunavut. In Summary of Activities 2020, Canada-Nunavut Geoscience Office (pp. 63–72).

Lesack, L. F., & Marsh, P. (2010). River-to-lake connectivities, water renewal, and aquatic habitat diversity in the Mackenzie River Delta. Water Resources Research, 46(12), W12504.

MacDonald, L. A., Gibson, J. J., & Reid, R. (2017). Assessing evaporation in a cold region wetland using stable isotopes. Hydrological Processes, 31(14), 2639–2651.

McMartin, I. (2000). Till composition across the Meliadine Trend, Rankin Inlet Area, Kivalliq region, Nunavut. Geological Survey of Canada, Open File 3747.

McMartin, I. (2002). Surficial geology, Rankin Inlet, Nunavut. Geological Survey of Canada, Open File 4116, scale 1:50 000. https://doi.org/10.4095/213219

McMartin, I., Gauthier, M. S., & Page, A. V. (2023). Updating the limits of the postglacial marine transgression along western Hudson Bay in Nunavut and Manitoba, Canada. INQUA Congress 2023.

Meldrum, J. L., Jamieson, H. E., & Dyke, L. D. (2001). Oxidation of mine tailings from Rankin Inlet, Nunavut, at subzero temperatures. Canadian Geotechnical Journal, 38(5), 957–966.

Millero, F. J., Feistel, R., Wright, D. G., & McDougall, T. J. (2008). The composition of Standard Seawater and the definition of the Reference-Composition Salinity Scale. Deep-Sea Research Part I, 55(1), 50–72.

Mongeau, P. (2014). Géochimie isotopique du soufre des minéralisations aurifères orogéniques du district de Meliadine, Nunavut (Master's thesis). Université Laval, Québec, 132 pp.

Muster, S., Roth, K., Langer, M., Lange, S., Cresto Aleina, F., Bartsch, A., ... & Boike, J. (2017). PeRL: A circum-Arctic Permafrost Region Pond and Lake database. Earth System Science Data, 9(1), 317–348. https://doi.org/10.5194/essd-9-317-2017

Parkhurst, D. L., & Appelo, C. A. J. (2013). Description of Input and Examples for PHREEQC Version 3: A Computer Program for Speciation, Batch-Reaction, One-Dimensional Transport, and Inverse Geochemical Calculations. U.S. Geological Survey Techniques and Methods, Book 6, Chapter A43.

Pasche, N., Schmid, M., Vazquez, F., Schubert, C. J., Wüest, A., Kessler, J. D., ... & Bürgmann, H. (2011). Methane sources and sinks in Lake Kivu. Journal of Geophysical Research: Biogeosciences, 116(G3), G03006.

Quay, P. D., Emerson, S. R., Quay, B. M., & Devol, A. H. (1986). The carbon cycle for Lake Washington—A stable isotope study. Limnology and Oceanography, 31(3), 596–611.

Randour, I., McMartin, I., & Roy, M. (2016). Study of the postglacial marine limit between Wager Bay and Chesterfield Inlet, western Hudson Bay, Nunavut. In Canada-Nunavut Geoscience Office Summary of Activities (pp. 51–60).

Skrzypek, G., Mydłowski, A., Dogramaci, S., Hedley, P., Gibson, J. J., & Grierson, P. F. (2015). Estimation of evaporative loss based on the stable isotope composition of water using Hydrocalculator. Journal of Hydrology, 523, 781–789. https://doi.org/10.1016/j.jhydrol.2015.02.010

St-Jean, G. (2003). Automated quantitative and isotopic (13C) analysis of dissolved inorganic carbon and dissolved organic carbon in continuous-flow using a total organic carbon analyser. Rapid Communications in Mass Spectrometry 17, 419–428.

Terzer-Wassmuth, S., Araguás-Araguás, L. J., Copia, L., et al. (2022). High spatial resolution prediction of tritium (^{3}H) in contemporary global precipitation. Scientific Reports, 12, 10271. https://doi.org/10.1038/s41598-022-14227-5

Turner, K. W., Wolfe, B. B., Edwards, T. W. D., Lantz, T. C., Hall, R. I., & Larocque, G. (2014). Controls on water balance of shallow thermokarst lakes and their relations with catchment characteristics: A multiyear, landscape-scale assessment based on water isotope tracers and remote sensing in Old Crow Flats, Yukon (Canada). Hydrological Processes, 28(14), 4161–4177.

Vet, R., Artz, R. S., Carou, S., Shaw, M., Ro, C. U., Aas, W., Baker, A., et al. (2014). A global assessment of precipitation chemistry and deposition of sulfur, nitrogen, sea salt, base cations, organic acids, acidity and pH, and phosphorus. Atmospheric Environment, 93, 3–100. https://doi.org/10.1016/j.atmosenv.2013.10.060

Vincent, W. F., Mueller, D. R., & Van Hove, P. (2011). Arctic lakes and rivers. In Polar Lakes and Rivers (pp. 27–51). Oxford University Press.

Welch, H. E., & Legault, J. A. (1986). Precipitation chemistry and chemical limnology of fertilized and natural lakes at Saqvaqjuac, N.W.T. Canadian Journal of Fisheries and Aquatic Sciences, 43, 2135–2145.

FIGURES

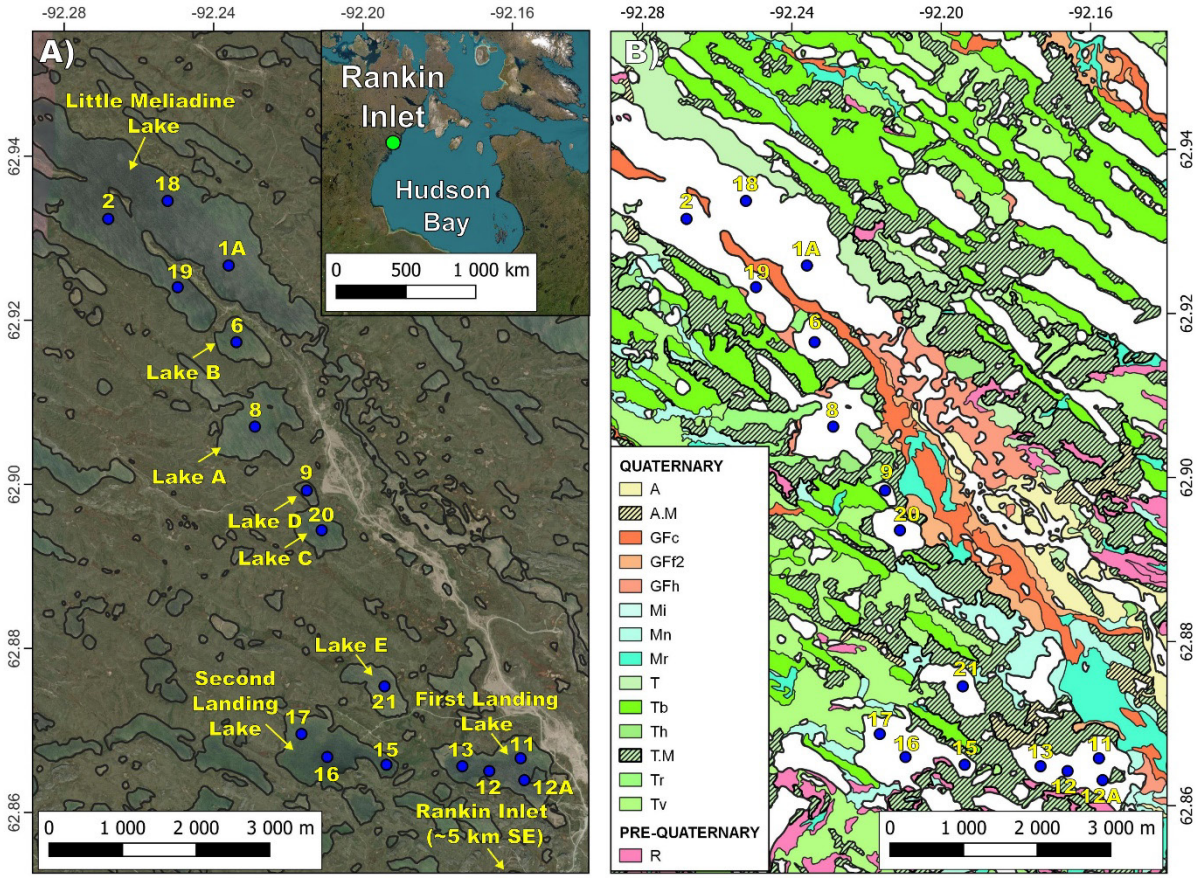

Figure 1: A) Location map of sampled lentic basins near Rankin Inlet (Nunavut, Canada) during the September 2023 field season. The background is a 0.46m *MAXAR Vivid* image (September 3rd, 2022) of the area of interest.; B) Surficial geology of the study area (data from Geological Survey of Canada, 2017 & McMartin, 2023). Unit abbreviations: A - alluvial sediments; GFc - ice-contact glaciofluvial sediments; Gff2 - outwash-fan glaciofluvial sediments; Mi - intertidal marine sediments; Mn - littoral/near-shore marine sediments; Mr - beach-ridge marine sediments; Tb - blanket till; Th – hummocky till; Tr - moraine-ridge till; Tv - till veneer; R - bedrock. Note: "M" indicates a secondary marine component superimposed on the main unit and shown as hatching in Panel B (e.g., A.M = alluvium with marine influence; T.M = till with marine influence).

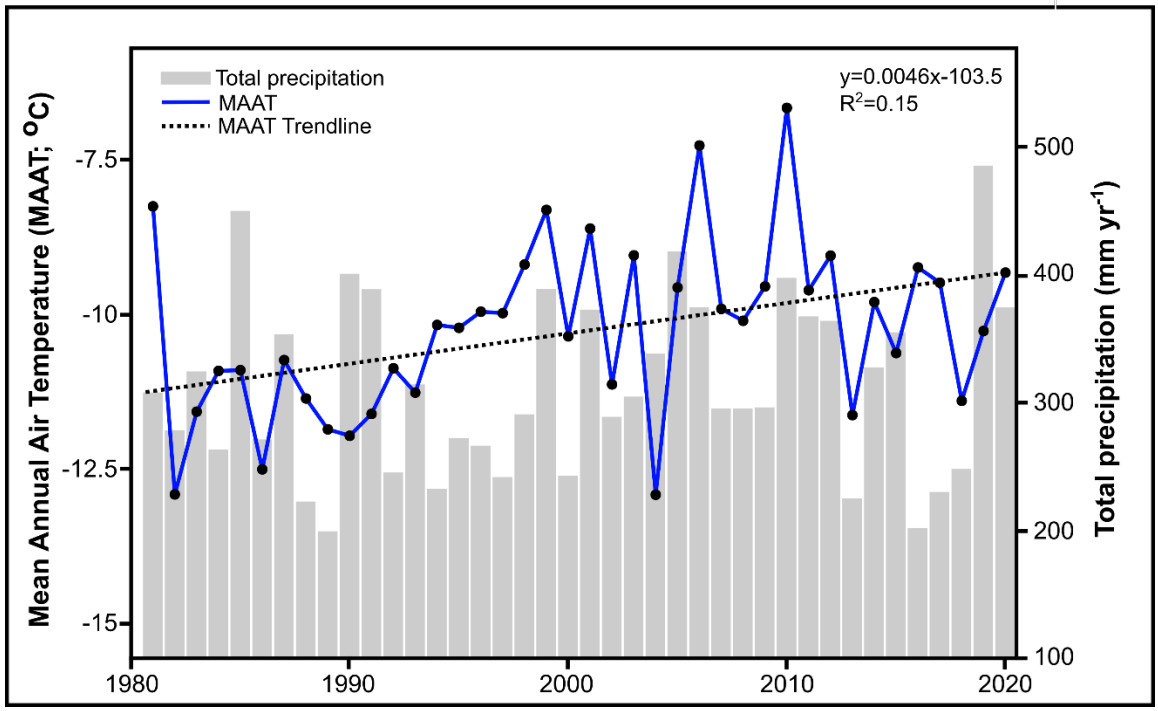

Figure 2: Time-series line and bar chart showing Rankin Inlet's Mean Annual Air Temperature (MAAT; °C) and total precipitation (mm yr^{-1}) during the 1981-2020 period. Data were taken from the Government of Canada's Historical Climate Data website (https://climate.weather.gc.ca/index_e.html). Figure from Faucher et al. (2022).

Figure 3: September 2023 field photographs of: A) UAV pilot É. Girard preparing a DJI Matrice 300 RTK Unmanned Aerial Vehicle (UAV), drone for planned aerial water sampling missions near Rankin Inlet, Nunavut; and B) collection of water samples from a *Speedip* device, ensuring transfer into well-sealed HDPE or glass bottles for subsequent geochemical analysis.

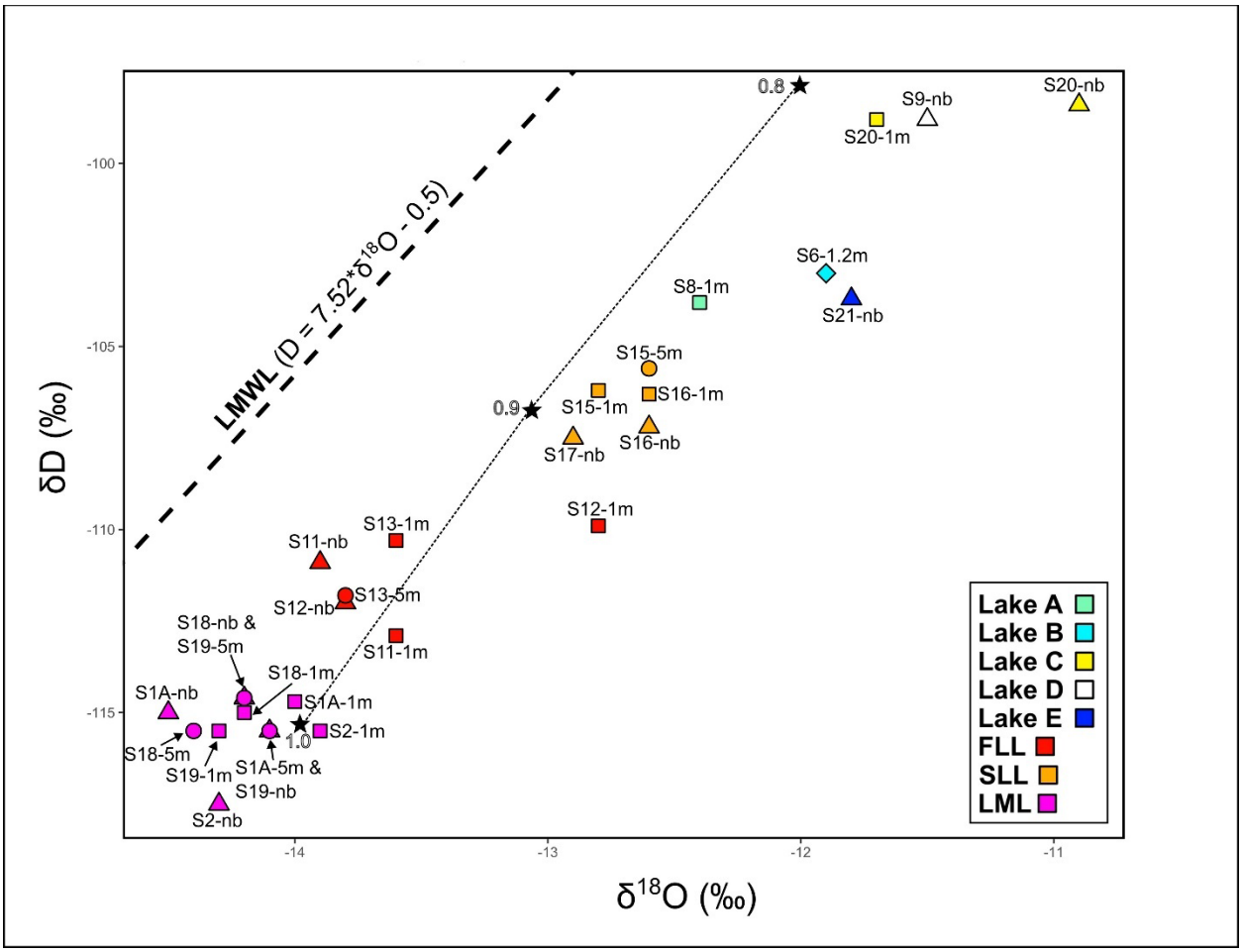

Figure 4: Stable water isotope co-plot of lake water samples taken at various sites in the water columns of Lake A-E, First Landing Lake (FLL), Second Landing Lake (SLL), and Little Meliadine Lake (LML). Squares represent samples taken at 1 m below the surface, while those collected 5 m below the surface are shown as circles. Triangles indicate samples taken near the bottom of the lake. The local meteoric water line (LMWL) from Churchill (Manitoba) is also included for comparative purposes. A black dashed line with stars represents a simulated lake water evaporation trend, assuming an initial composition similar to the largest sampled lake (LML), which is expected to largely retain a meteoric water signature due to its lower susceptibility to evaporation compared to smaller basins. The numbers next to the stars (1.0, 0.9, and 0.8) indicate the residual water content under the evaporation simulation performed in the *PHREEQC* software.

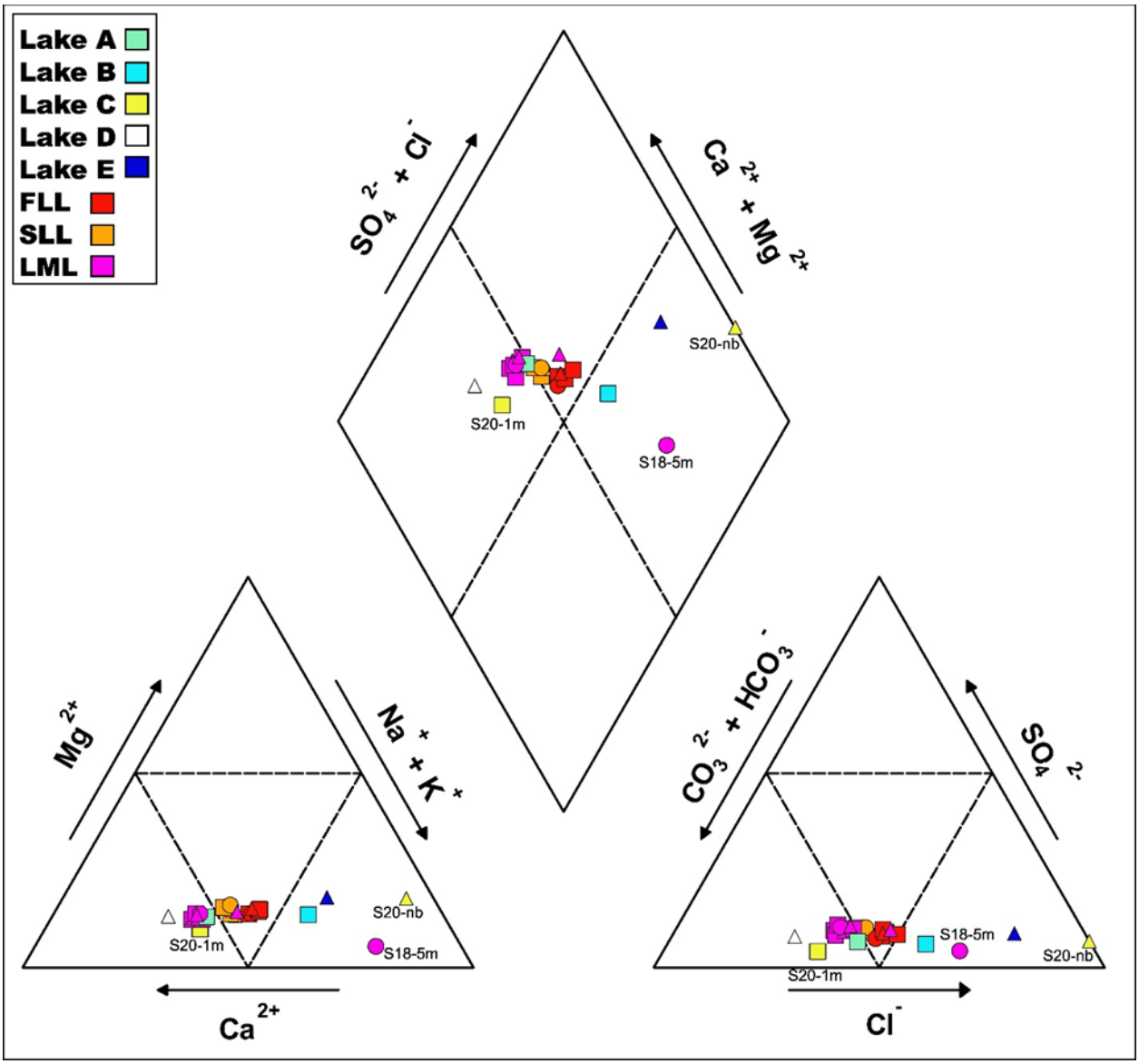

Figure 5: Ternary diagrams of major dissolved cations and anions in samples collected from the water columns of Lake A-E, First Landing Lake (FLL), Second Landing Lake (SLL) and Little Meliadine Lake (LML). Squares represent samples taken at 1 m below the surface, while those collected at 5 m below the surface are shown as circles. Triangles indicate samples taken near the bottom of the lake. The near-bottom sample from site 20 is highlighted for its distinct geochemical composition relative to its near-surface (1 m) counterpart, and the 5 m depth sample from site 18 at FLL is emphasized due to its unique signature compared to the remainder of the water column. In contrast, all other sites exhibit similar geochemical compositions with depth.

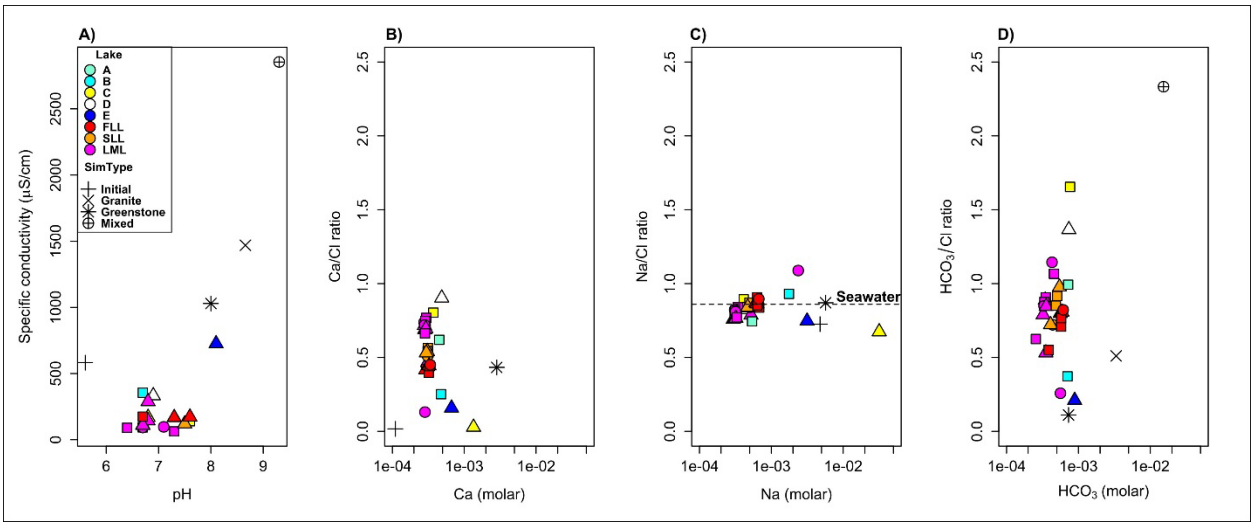

Figure 6: Comparison of measured lake-water compositions with PHREEQC-simulated weathering results using regional till units mixed with atmospherically equilibrated precipitation (99 %) and sea-spray aerosols (1 %; values from Millero et al., 2008). The four panels display: A) pH versus specific conductance, B) Ca (mol) versus Ca/Cl (molar ratio), C) Na (mol) versus Na/Cl (molar ratio), and D) HCO_3 (mol) versus HCO_3/Cl (molar ratio). The Y axis in panels (B), (C), and (D) is plotted on a logarithmic scale. In panel (B), Ca/Cl values for the granite-rich and mixed-till simulations fall below the lower axis limit (1×10^{-4}), as do Na/Cl values for the granite-rich scenario in panel (C). A horizontal reference line at Na/Cl = 0.86 is included in panel (C) to represent the open-ocean seawater molar ratio. Lake-water samples collected at 1 m, 5 m, and near-bottom (nb) depths are shown as squares, circles, and triangles, respectively. Simulated water compositions are represented as follows: plus signs for the initial precipitation–sea-spray input, diagonal crosses for the granite-rich scenario, asterisk-like symbols for greenstone-rich weathering, and circles with a central cross for the mixed granite-greenstone simulation. Simulation results and lake chemistry data are provided in Table A1 (Appendix).

TABLES

Table 1: Summary of physicochemical (temperature, specific conductivity, pH) and hydrochemical (solute concentrations and isotopic ratios) properties of water samples collected at various sites and depths in lentic basins near Rankin Inlet, Nunavut, in September 2023. Lakes (and associated sites) are presented in order of decreasing maximum depth, with the deepest basins listed first. Surface area (SA) and maximum depth (MD) are indicated for each lake. Conductivity values from Faucher et al. (2024) were standardized to specific conductivity at 25 °C using a temperature-correction procedure that adjusts raw conductivity by approximately 2% per degree Celsius difference from 25 °C.

Lakes/Sites	Temp. (°C)	Spec. cond. (uS/ cm^{-1})	pH	Ca (mg/L)	K (mg/L)	Mg (mg/L)	Na (mg/L)	Cl (mg/L)	SO_4 (mg/L)	HCO_3 (mg/L)	$\delta^{18}O$ (‰)	d (‰)	^{3}H (TU)	$\delta^{13}C$ (‰)	^{34}S-SO_4 (‰)
First Landing Lake (SA=0.89 km^2, MD≥7.6)															
S12-1 m	6.9	174	6.7	11.8	2	2.5	14.6	24.8	6.5	23.5	-12.8	-7.1	NA	-5.4	NA
S12-nb (16.6 m)	7.6	172	7.6	11.7	1.7	2.4	14	24.8	6.1	34.1	-13.8	-1.5	NA	-5.3	3.8
S11-1 m	NA	NA	7.3	12.9	2.1	2.8	15.6	28.7	6.3	35	-13.6	-4.4	NA	-5	NA
S11-nb (3.6 m)	7.7	168	7.3	13	1.8	2.7	14.5	25.9	6	36	-13.9	0.3	10.9±0.7	-5.2	0.7
S13-1 m	NA	NA	7.2	13.3	1.9	2.7	14.7	26.6	5.9	35.1	-13.6	-1.6	NA	-5.1	NA
S13-5 m	NA	NA	7.2	13.5	1.9	2.7	15.4	26.5	5.9	37.5	-13.8	-1.4	10.9±0.7	-5.3	0.9
Little Meliadine Lake (SA=5.27 km^2, MD≥17.3)															
S18-1 m	9.5	90	6.4	11.7	1.4	1.6	7.9	14.5	4.4	15.6	-14.2	-1.1	NA	-5.4	NA
S18-5 m	9.1	92	6.7	11.4	5.5	2	54.5	77.2	6.4	34.3	-14.4	-0.5	NA	-5.1	5.1
S18-nb (17.3 m)	8.7	288	6.8	11.2	1.2	1.5	6.8	13.8	4.3	21.1	-14.2	-1	10.6±0.7	-4.6	4.5
S19-1 m	8.8	95	6.7	11.9	1.3	1.5	7.1	13.7	4.3	21.4	-14.3	-1.1	NA	-4.6	NA
S19-5 m	8.5	97	7.1	11.1	1.3	1.4	7.1	13.3	4.2	26.2	-14.2	-0.9	NA	-4.4	4.9
S19-nb (7.1 m)	8.4	112	6.7	11.3	1.3	1.6	7.2	14.5	4.5	19.7	-14.1	-2.5	10.6±0.7	-5.7	5.3
S1A-1 m	8.3	93	6.7	11.5	1.2	1.5	7.2	13.6	4.5	20.5	-14	-2.3	NA	-4.8	NA
S1A-5 m	8.3	93	6.7	11.3	1.3	1.5	7.3	13.9	4.3	20.3	-14.1	-2.5	NA	-4.7	NA
S1A-nb (8.5 m)	8.9	143	6.8	11.7	1.3	1.5	7.4	14.9	4.3	21.7	-14.5	1.2	NA	-6.3	6
S2-1 m	10.1	63	7.3	11.4	1.3	1.5	7.6	15.2	4.3	27.9	-13.9	-4.1	NA	-5.2	6.7
S2-nb (12.3 m)	8.5	109	6.7	12.4	1.6	2.1	12	23.5	5.2	21.5	-14.3	-2.9	9.9±0.6	-6.9	9.5
Second Landing Lake															

(SA=0.94 km^2, MD≥7.2)															
S15-1 m	NA	NA	7.1	12.5	1.7	2.2	10.7	19.6	5.5	30.9	-12.8	-4.1	NA	-5.6	NA
S15-5 m	NA	NA	6.9	12.4	1.6	2.4	11.7	21.5	5.5	26.7	-12.6	-5	11.2±0.7	-6.1	0.8
S16-1 m	NA	NA	7	12.4	1.6	2.1	11.4	20.2	5.4	29.6	-12.6	-5.8	NA	-6.1	NA
S16-nb (4.8 m)	NA	NA	6.8	12.3	1.8	2.2	10.9	20.1	5.5	25	-12.6	-6	11.3±0.7	-7.2	2.1
S17-nb (1.7 m)	7.8	120	7.5	11.9	1.6	2.1	10.8	19.8	5.4	33.3	-12.9	-4.3	10.8±0.7	-5.8	1.9
Lake C (SA=0.30 km^2, MD≥3.13)															
S20-1 m	8.3	140	7.6	14.9	2	1.7	9.5	16.4	2.9	46.7	-11.7	-5.4	NA	-5	NA
S20-nb (3.1 m)	7.8	169	6.8	54	23.8	94.3	729.3	1668	172.2	0	-10.9	-11	10.8±0.7	-10	NA
Lake A (SA=0.99 km^2, MD≥1.79)															
S8-1 m	NA	NA	7.2	18	2.2	2.6	12.4	25.7	5.3	43.9	-12.4	-4.3	NA	-4.8	NA
Lake D (SA=0.06 km^2, MD≥1.40															
S9-nb (1.4 m)	8	333	6.9	19.5	2.7	2.4	10.2	19.1	5	44.9	-11.5	-6.7	NA	-3.6	NA
Lake B (SA=0.31 km^2, MD≥1.20)															
S6-1 m	7	355	6.7	19.1	3.4	5.6	40.5	67.1	9.6	43	-11.9	-8.1	NA	-3.5	2.8
Lake E (SA=0.36 km^2, MD≥1.15)															
S21-nb (1.2 m)	8.6	726	8.1	26.7	4.7	11.7	72.3	149.2	21.2	54.1	-11.8	-9.2	11.8±0.7	-5.9	16.7

APPENDIX

Table A1: Simulated geochemical evolution of snowmelt mixed with marine aerosols and weathered granite, greenstone, and mixed tills under open system weathering conditions.

Simulations & Lake data	pH	Spec. Condc. uS cm^{-1}	Ca^{2+} (mol/L)	Na^{+} (mol/L)	Mg^{2+} (mol/L)	Cl^{-} (mol/L)	HCO_3^{-} (mol/L)	Ca/Cl (mol)	Na/Cl (mol)	HCO_3/Cl (mol)
Precipitation (Saqvaqjuac snow+Sea sprays)	5.6	582	1.10E-04	4.76E-03	5.43E-04	5.56E-03	NA	1.98E-02	8.57E-01	NA
Granite+Marine deposits	8.7	1469	1.91E-05	7.79E-12	8.92E-04	6.56E-03	3.35E-03	2.92E-03	1.19E-09	5.11E-01
Greenstone+Marine deposits	8	1029	2.84E-03	5.71E-03	9.35E-24	6.56E-03	7.29E-04	4.33E-01	8.71E-01	1.11E-01
Greenstone+Granite	9.3	2854	1.79E-09	1.91E-08	1.21E-22	6.56E-03	1.53E-02	2.72E-07	2.92E-06	2.34E+00
First Landing Lake										
S12-1 m	6.7	174	2.94E-04	6.35E-04	1.03E-04	7.00E-04	3.85E-04	4.21E-01	9.08E-01	5.51E-01
S12-nb (16.6 m)	7.6	172	2.92E-04	6.09E-04	9.87E-05	7.00E-04	5.59E-04	4.17E-01	8.71E-01	7.99E-01
S11-1 m	7.3	NA	3.22E-04	6.79E-04	1.15E-04	8.10E-04	5.74E-04	3.98E-01	8.38E-01	7.09E-01
S11-nb (3.6 m)	7.3	168	3.24E-04	6.31E-04	1.11E-04	7.31E-04	5.90E-04	4.44E-01	8.63E-01	8.08E-01
S13-1 m	7.2	NA	3.32E-04	6.39E-04	1.11E-04	7.50E-04	5.75E-04	4.42E-01	8.52E-01	7.67E-01
S13-5 m	7.2	NA	3.37E-04	6.70E-04	1.11E-04	7.47E-04	6.15E-04	4.51E-01	8.96E-01	8.22E-01
Little Meliadine Lake										
S18-1 m	6.4	90	2.92E-04	3.44E-04	6.58E-05	4.09E-04	2.56E-04	7.14E-01	8.40E-01	6.25E-01
S18-5 m	6.7	92	2.84E-04	2.37E-03	8.23E-05	2.18E-03	5.62E-04	1.31E-01	1.09E+00	2.58E-01
S18-nb (17.3 m)	6.8	288	2.79E-04	2.96E-04	6.17E-05	3.89E-04	3.46E-04	7.18E-01	7.60E-01	8.88E-01
S19-1 m	6.7	95	2.97E-04	3.09E-04	6.17E-05	3.86E-04	3.51E-04	7.68E-01	7.99E-01	9.08E-01
S19-5 m	7.1	97	2.77E-04	3.09E-04	5.76E-05	3.75E-04	4.29E-04	7.38E-01	8.23E-01	1.14E+00
S19-nb (7.1 m)	6.7	112	2.82E-04	3.13E-04	6.58E-05	4.09E-04	3.23E-04	6.89E-01	7.66E-01	7.89E-01

S1A-1 m	6.7	93	2.87E-04	3.13E-04	6.17E-05	3.84E-04	3.36E-04	7.48E-01	8.16E-01	8.76E-01
S1A-5 m	6.7	93	2.82E-04	3.18E-04	6.17E-05	3.92E-04	3.33E-04	7.19E-01	8.10E-01	8.49E-01
S1A-nb (8.5 m)	6.8	143	2.92E-04	3.22E-04	6.17E-05	4.20E-04	3.56E-04	6.95E-01	7.66E-01	8.46E-01
S2-1 m	7.3	63	2.84E-04	3.31E-04	6.17E-05	4.29E-04	4.57E-04	6.63E-01	7.71E-01	1.07E+00
S2-nb (12.3 m)	6.7	109	3.09E-04	5.22E-04	8.64E-05	6.63E-04	3.52E-04	4.67E-01	7.87E-01	5.32E-01
Second Landing Lake										
S15-1 m	7.1	NA	3.12E-04	4.65E-04	9.05E-05	5.53E-04	5.06E-04	5.64E-01	8.42E-01	9.16E-01
S15-5 m	6.9	NA	3.09E-04	5.09E-04	9.87E-05	6.06E-04	4.38E-04	5.10E-01	8.39E-01	7.22E-01
S16-1 m	7	NA	3.09E-04	4.96E-04	8.64E-05	5.70E-04	4.85E-04	5.43E-01	8.70E-01	8.51E-01
S16-nb (4.8 m)	6.8	NA	3.07E-04	4.74E-04	9.05E-05	5.67E-04	4.10E-04	5.41E-01	8.36E-01	7.23E-01
S17-nb (1.7 m)	7.5	120	2.97E-04	4.70E-04	8.64E-05	5.58E-04	5.46E-04	5.32E-01	8.41E-01	9.77E-01
Lake C										
S20-1 m	7.6	140	3.72E-04	4.13E-04	6.99E-05	4.63E-04	7.65E-04	8.04E-01	8.93E-01	1.65E+00
S20-nb (3.1 m)	6.8	169	1.35E-03	3.17E-02	3.88E-03	4.70E-02	0.00E+00	2.86E-02	6.74E-01	0.00E+00
Lake A										
S8-1 m	7.2	NA	4.49E-04	5.39E-04	1.07E-04	7.25E-04	7.19E-04	6.20E-01	7.44E-01	9.93E-01
Lake D										
S9-nb (1.4 m)	6.9	333	4.87E-04	4.44E-04	9.87E-05	5.39E-04	7.36E-04	9.03E-01	8.24E-01	1.37E+00
Lake B										
S6-1 m	6.7	355	4.77E-04	1.76E-03	2.30E-04	1.89E-03	7.05E-04	2.52E-01	9.31E-01	3.72E-01
Lake E										
S21-nb (1.2 m)	8.1	726	6.66E-04	3.14E-03	4.81E-04	4.21E-03	8.87E-04	1.58E-01	7.47E-01	2.11E-01